

1 High-order cognition is supported by information-rich but
2 compressible brain activity patterns

Lucy L. W. Owen^{1,2} and Jeremy R. Manning^{1,*}

¹Department of Psychological and Brain Sciences,
Dartmouth College, Hanover, NH

²Carney Institute for Brain Sciences,
Brown University, Providence, RI

* Address correspondence to jeremy.r.manning@dartmouth.edu

March 16, 2023

Abstract

We applied dimensionality reduction algorithms and pattern classifiers to functional neuroimaging data collected as participants listened to a story, temporally scrambled versions of the story, or underwent a resting state scanning session. These experimental conditions were intended to require different depths of processing and inspire different levels of cognitive engagement. We considered two primary aspects of the data. First, we treated the maximum achievable decoding accuracy across participants as an indicator of the “informativeness” of the recorded patterns. Second, we treated the number of features (components) required to achieve a threshold decoding accuracy as a proxy for the “compressibility” of the neural patterns (where fewer components indicate greater compression). Overall, we found that the peak decoding accuracy (achievable without restricting the numbers of features) was highest in the intact (unscrambled) story listening condition. However, the number of features required to achieve comparable classification accuracy was also lowest in the intact story listening condition. Taken together, our work suggests that our brain networks flexibly reconfigure according to ongoing task demands, and that the activity patterns associated with higher-order cognition and high engagement are both more informative and more compressible than the activity patterns associated with lower-order tasks and lower levels of engagement.

Keywords: information, compression, temporal decoding, dimensionality reduction, neuroimaging

²⁴ Introduction

25 Large-scale networks, including the human brain, may be conceptualized as occupying one or
26 more positions along on a continuum. At one extreme, every node is fully independent from
27 every other node. At the other extreme, all nodes behave identically. Each extreme optimizes
28 key properties of how the network functions. When every node is independent, the network is

29 maximally *expressive*: if we define the network’s “state” as the activity pattern across its nodes, then
30 every state is equally reachable by a network with fully independent nodes. On the other hand, a
31 network of identically behaved nodes optimizes *robustness*: any subset of nodes may be removed
32 from the network without any loss of function or expressive power, as long as any single node
33 remains. Presumably, most natural systems tend to occupy positions between these extremes. We
34 wondered: might the human brain reconfigure itself to be more flexible or more robust according
35 to ongoing demands? In other words, might the brain reconfigure its connections or behaviors
36 under different circumstances to change its position along this continuum?

37 Closely related to the above notions of expressiveness versus robustness are measures of
38 how much *information* is contained in a given signal or pattern, and how *redundant* a signal
39 is (Shannon, 1948). Formally, information is defined as the amount of uncertainty about a given
40 variables’ outcomes (i.e., entropy), measured in *bits*, or the optimal number of yes/no questions
41 needed to reduce uncertainty about the variable’s outcomes to zero. Highly complex systems with
42 many degrees of freedom (i.e., high flexibility and expressiveness), are more information-rich than
43 simpler or more constrained systems. The redundancy of a signal denotes the difference between
44 how expressive the signal *could* be (i.e., proportional to the number of unique states or symbols
45 used to transmit the signal) and the actual information rate (i.e., the entropy of each individual
46 state or symbol). If a brain network’s nodes are fully independent, then the number of bits required
47 to express a single activity pattern is proportional to the number of nodes. The network would
48 also be minimally redundant, since the status of every node would be needed to fully express a
49 single brain activity pattern. If a brain network’s nodes are fully coupled and identical, then the
50 number of bits required to express a single activity pattern is proportional to the number of unique
51 states or values any individual node can take on. Such a network would be highly redundant,
52 since knowing any individual node’s state would be sufficient to recover the full-brain activity
53 pattern. Highly redundant systems are also robust, since there is little total information loss due
54 to removing any given observation.

55 We take as a given that brain activity is highly flexible: our brains can exhibit nearly infinite
56 varieties of activity patterns. This flexibility implies that our brains activity patterns are highly
57 information rich. However, brain activity patterns are also highly structured. For example,
58 full-brain correlation matrices are stable within (Finn et al., 2017, 2015; Gratton et al., 2018) and

59 across (Cole et al., 2014; Glerean et al., 2012; Gratton et al., 2018; Yeo et al., 2011) individuals. This
60 stability suggests that our brains' activity patterns are at least partially constrained, for example
61 by anatomical, external, or internal factors. Constraints on brain activity that limit its flexibility
62 decrease expressiveness (i.e., its information rate). However, constraints on brain activity also
63 increase its robustness to noise (e.g., "missing" or corrupted signals may be partially recovered).
64 For example, recent work has shown that full-brain activity patterns may be reliably recovered
65 from only a relatively small number of implanted electrodes (Owen et al., 2020; Scangos et al.,
66 2021). This robustness property suggests that the relevant signal (e.g., underlying factors that
67 have some influence over brain activity patterns) are compressible.

68 To the extent that brain activity patterns contain rich task-relevant information, we should be
69 able to use the activity patterns to accurately differentiate between different aspects of a task (e.g.,
70 using pattern classifiers; Norman et al., 2006). For example, prior work has shown a direct
71 correspondence between classification accuracy and the information content of a signal (Alvarez,
72 2002). To the extent that brain activity patterns are compressible, we should be able to generate
73 simplified (e.g., lower dimensional) representations of the data while still preserving the relevant
74 or important aspects of the original signal. In general, information content and compressibility are
75 related but are partially dissociable (Fig. 1). If a given signal (e.g., a representation of brain activity
76 patterns) contains more information about ongoing cognitive processes, then the peak decoding
77 accuracy should be high. And if the signal is compressible, a low-dimensional embedding of the
78 signal will be similarly informative as the original signal (Fig. 1D).

79 Several recent studies suggest that the complexity of brain activity is task-dependent, whereby
80 simpler tasks with lower cognitive demands are reflected by simpler and more compressible brain
81 activity patterns, and more complex tasks with higher cognitive demands are reflected by more
82 complex and less compressible brain activity patterns (Mack et al., 2020; Owen et al., 2021). These
83 findings complement other work suggesting that functional connectivity (correlation) patterns are
84 task-dependent (Cole et al., 2014; Finn et al., 2017; Owen et al., 2020), although see Gratton et
85 al. (2018). Higher-order cognitive processing of a common stimulus also appears to drive more
86 stereotyped task-related activity and functional connectivity across individuals (Hasson et al.,
87 2008; Lerner et al., 2011; Simony & Chang, 2020; Simony et al., 2016).

88 The above studies are consistent with two potential descriptions of how cognitive processes are

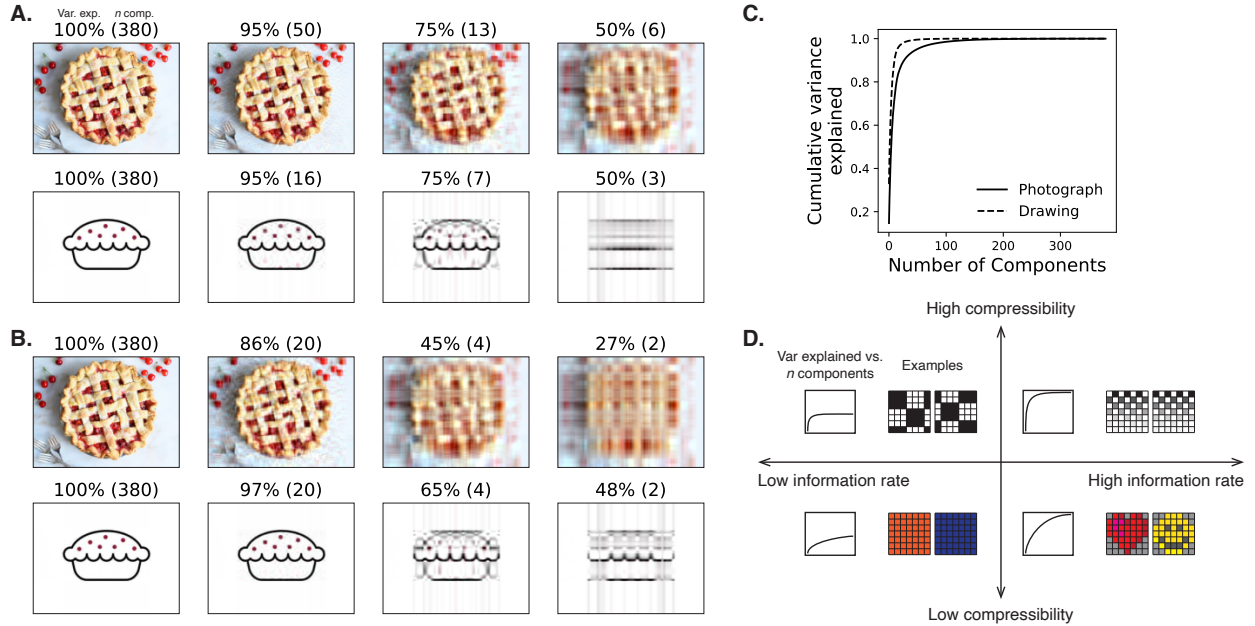


Figure 1: Information content and compressibility. **A. Variance explained for two images.** We applied principal components analysis to a photograph and drawing, treating the rows of the images as “observations.” Across columns, we identified the numbers of components required to explain 100%, 95%, 75%, or 50% of the cumulative variance in each image (the 100% columns denote the original images). The numbers of components are indicated in parentheses, and the resulting “compressed” images are displayed. **B. Representing two images with different numbers of components.** Using the same principal component decompositions as in Panel A, we computed the cumulative proportion of variance explained with 380 (original images), 20, 4, or 2 components. **C. Cumulative variance explained versus number of components.** For the images displayed in Panels A and B, we plot the cumulative proportion of variance explained as a function of the number of components used to represent each image. **D. Information rate and compressibility.** Across multiple images, the information rate (i.e., the amount of information contained in each image; horizontal axis) is high when each individual pixel provides information that cannot be inferred from other pixels. High-information rate images tend to be high-resolution, and low-information rate images tend to be low-resolution. Compressibility is related to the difference between the information required to specify the original versus compressed images (vertical axis). Highly compressible images often contain predictable structure (redundancies) that can be leveraged to represent the images much more efficiently than in their original feature spaces.

89 reflected in brain activity patterns. One possibility is that the information rate of brain activity in-
90 creases during more complex or higher-level cognitive processing. If so, then the ability to reliably
91 decode cognitive states from brain activity patterns should improve with task complexity or with
92 the level (or “depth”) of cognitive processing. A second possibility is that the compressibility of
93 brain activity patterns increases during more complex or higher-level cognitive processing. If so,
94 then individual features of brain recordings, or compressed representations of brain recordings,
95 should carry more information during complex or high-level (versus simple or low-level) cognitive
96 tasks.

97 We used a previously collected neuroimaging dataset to estimate the extent to which each of
98 these two possibilities might hold. The dataset we examined comprised functional magnetic reso-
99 nance imaging (fMRI) data collected as participants listened to an audio recording of a 10-minute
100 story, temporally scrambled recordings of the story, or underwent a resting state scan (Simony
101 et al., 2016). Each of these experimental conditions evokes different depths of cognitive process-
102 ing (Hasson et al., 2008; Lerner et al., 2011; Owen et al., 2021; Simony et al., 2016). We used
103 across-participant classifiers to decode listening times in each condition, as a proxy for how “infor-
104 mative” the task-specific activity patterns were (Simony & Chang, 2020). We also used principle
105 components analysis to generate lower-dimensional representations of the activity patterns. We
106 then repeated the classification analyses after preserving different numbers of components and
107 examined how classification accuracy changed across the different experimental conditions.

108 Results

109 We sought to understand whether higher-level cognition is reflected by more reliable and in-
110 formative brain activity patterns, and how compressibility of brain activity patterns relates to
111 cognitive complexity. We developed a computational framework for systematically assessing the
112 informativeness and compressibility of brain activity patterns recorded under different cognitive
113 circumstances. We used across-participant decoding accuracy (see *Forward inference and decoding*
114 *accuracy*) as a proxy for informativeness. To estimate the compressibility of the brain patterns, we
115 used group principal components analysis (PCA) to project the brain patterns into k -dimensional
116 spaces, for different values of k (see *Hierarchical Topographic Factor Analysis (HTFA)* and *Principal*

117 components analysis (PCA)). For more compressible brain patterns, decoding accuracy should be
118 more robust to small values of k .

119 We analyzed a dataset collected by Simony et al. (2016) that comprised four experimental
120 conditions. These conditions exposed participants to stimuli that systematically varied in cognitive
121 engagement. In the *intact* experimental condition, participants listened to an audio recording of
122 a 10-minute story. In the *paragraph*-scrambled experimental condition, participants listened to a
123 temporally scrambled version of the story, where the paragraphs occurred out of order, but where
124 the same set of paragraphs was presented over the entire listening interval. All participants in
125 this condition experienced the scrambled paragraphs in the same order. In the *word*-scrambled
126 experimental condition, participants listened to a temporally scrambled version of the story, where
127 the words occurred in a random order. Again, all participants in this condition experienced the
128 scrambled words in the same order. Finally, in the *rest* experimental condition, participants lay
129 in the scanner with no overt stimulus, while keeping their eyes open and blinking as needed.
130 This public dataset provided a convenient means for testing our hypothesis that different levels
131 of cognitive processing and engagement affect how informative and compressible the associated
132 brain patterns are.

133 To evaluate the relation between informativeness and compressibility for brain activity from
134 each experimental condition, we trained a series of across-participant temporal decoders on com-
135 pressed representations of the data. Figure 2A displays the decoding accuracy as a function
136 of the number of principal components used to represent the data (also see Fig. S1). Several
137 patterns were revealed by the analysis. First, in general (i.e., across experimental conditions),
138 decoding accuracy tends to improve as the number of components are increased. However, de-
139 coding accuracy peaked at higher levels for experimental conditions that exposed participants
140 to cognitively richer stimuli (Fig. 2D). The peak decoding accuracy was highest for the “intact”
141 condition (versus paragraph: $t(99) = 35.205, p < 0.001$; versus word: $t(99) = 43.172, p < 0.001$);
142 versus rest: $t(99) = 81.361, p < 0.001$), next highest for the “paragraph” condition (versus word:
143 $t(99) = 6.243, p < 0.001$; versus rest: $t(99) = 50.748, p < 0.001$), and next highest for the “word”
144 condition (versus rest: $t(99) = 48.791, p < 0.001$). This ordering implies that cognitively richer
145 conditions evoke more stable brain activity patterns across people.

146 The cognitively richer conditions also displayed steeper initial slopes. For example, the intact

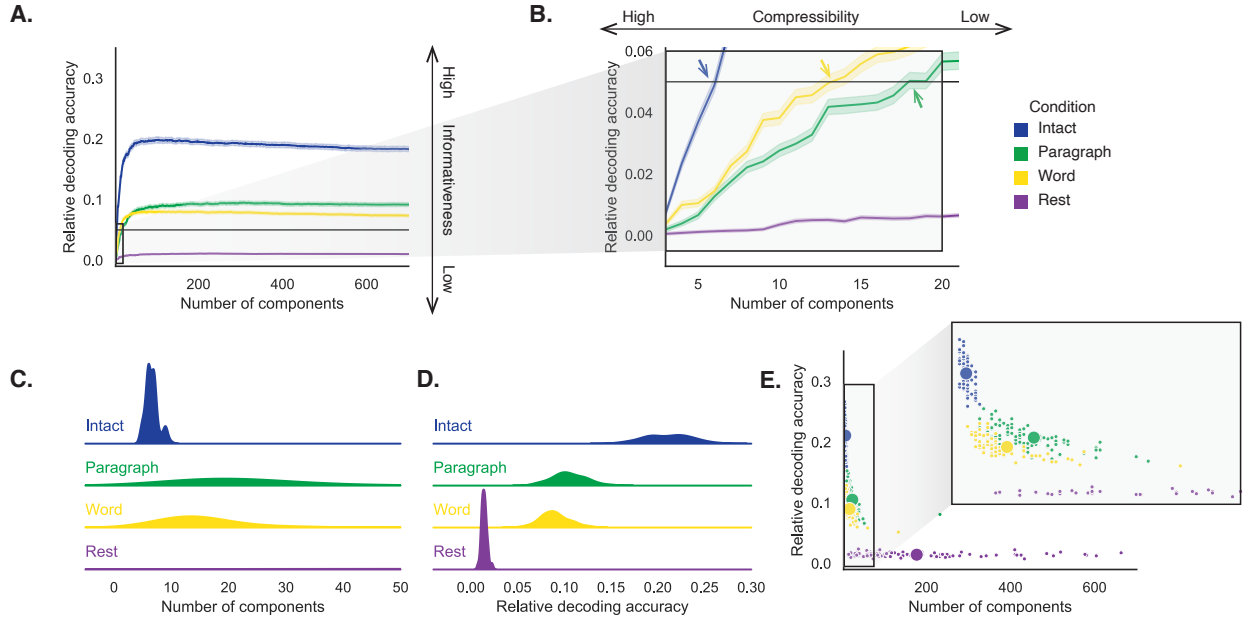


Figure 2: Decoding accuracy and compression. A. Decoding accuracy by number of components. Ribbons of each color display cross-validated decoding performance for each condition (intact, paragraph, word, and rest), as a function of the number of components (features) used to represent the data. For each condition, decoding accuracy has been normalized by subtracting expected “chance” decoding performance (estimated as $\frac{1}{T}$, where T is the number of timepoints in the given condition). This normalization was intended to enable fairer comparisons across conditions; a relative decoding accuracy of 0.0 denotes “chance” performance. The horizontal black line denotes 5% decoding accuracy (used as a reference in Panel B). **B. Numbers of components required to reach a fixed decoding accuracy threshold, by condition.** The panel displays a zoomed-in view of the inset in Panel A. Intersections between each condition’s decoding accuracy curve and the 5% decoding accuracy reference line are marked by arrows. All error ribbons in Panels A and B denote bootstrap-estimated 95% confidence intervals. **C. Estimating “compressibility” for each condition.** The density plots display the numbers of components required to reach at least 5% (corrected) decoding accuracy, across all cross validation runs. For the “rest” condition, where decoding accuracy never reached 5% accuracy, we display the distribution of the numbers of components required to achieve the peak decoding accuracy in each fold. (This distribution is nearly flat, as also illustrated in Panel E.) **D. Estimating “informativeness” for each condition.** The density plots display the peak (corrected) decoding accuracies achieved in each condition, across all cross validation runs. **E. Informativeness versus compressibility.** Each dot displays the minimum number of components required to achieve at least 5% corrected decoding accuracy (x -coordinate; for the rest condition the numbers of components are estimated using the peak decoding accuracies as in Panel C) and the peak (corrected) decoding accuracy (y -coordinate). The smaller dots correspond to individual cross validation runs and the larger dots display the averages across runs. The inset displays a zoomed-in view of the indicated region in the main panel.

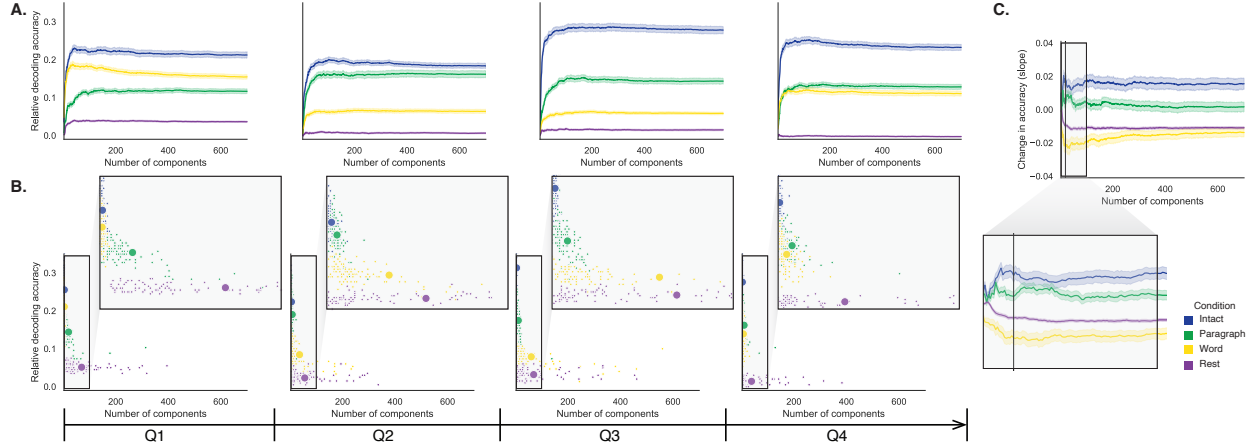


Figure 3: Changes in decoding accuracy and compression over time. **A. Decoding accuracy by number of components, by story segment.** Each family of curves is plotted in the same format as Figure 2A but reflects data only from one quarter of the dataset. **B. Informativeness versus compressibility by condition and segment.** Each scatter plot is in the same format as Figure 2E, but reflects data only from one quarter of the dataset. **C. Change in decoding accuracy over time, by number of components.** For each number of components (x -axis) and condition (color), we fit a regression line to the decoding accuracies obtained for the first, second, third, and fourth quarters of the dataset (corresponding to the columns of Panels A and B). The y -axis denotes the slopes of the regression lines. All error ribbons denote bootstrap-estimated 95% confidence intervals.

147 condition decoders reached an arbitrarily chosen threshold of 5% accuracy using fewer components
 148 than the paragraph condition decoders ($t(99) = -7.429, p < 0.001$) or word condition decoders
 149 ($t(99) = -7.300, p < 0.001$), and decoding accuracy never exceeded 5% for the rest condition. This
 150 suggests that brain activity patterns evoked by cognitively richer conditions are more compressible,
 151 such that representing the data using the same number of principal components provides more
 152 information to the temporal decoders (Figs. 2B, C). Taken together, as shown in Figure 2E, we
 153 found that brain activity patterns evoked by cognitively richer conditions tended to be both more
 154 informative (i.e., associated with higher decoding accuracies) *and* more compressible (i.e., requiring
 155 fewer components to achieve the 5% accuracy threshold).

156 If informativeness (to the temporal decoders) and compressibility vary with the cognitive
 157 richness of the stimulus, might these measures also vary over time *within* a given condition? For
 158 example, participants in the intact condition might process the ongoing story more deeply later
 159 on in the story (compared with earlier in the story) given the additional narrative background
 160 and context they had been exposed to by that point. To examine this possibility, we divided each
 161 condition into four successive time segments. We computed decoding curves (Fig. 3A) and the

162 numbers of components required to achieve 5% decoding accuracy (Fig. 3B) for each segment and
163 condition. We found that, in the two most cognitively rich conditions (intact and paragraph), both
164 decoding accuracy and compressibility, as reflected by the change in decoding curves, increased
165 with listening time (e.g., at the annotated reference point of $k = 20$ components in Fig. 3C: intact:
166 $t(99) = 7.915, p < 0.001$; paragraph: $t(99) = 2.354, p = 0.021$). These changes may reflect an increase
167 in comprehension or depth of processing with listening time. In contrast, the decoding accuracy
168 and compressibility *decreased* with listening time in the word condition ($t(99) = -10.747, p < 0.001$)
169 and rest condition ($t(99) = -22.081, p < 0.001$). This might reflect the depletion of attentional
170 resources in the less-engaging word and rest conditions.

171 We also wondered how informativeness and compressibility in the different experimental
172 conditions might vary across brain networks. We used a network parcellation identified by Yeo et
173 al. (2011) to segment the brain into seven distinct networks. The networks can be sorted (roughly)
174 in order from lower-level to higher-level cortex as follows (Figs. 4A–C): visual, somatomotor,
175 dorsal attention, ventral attention, limbic, frontoparietal, and default mode. Next, we computed
176 decoding curves separately for the activity patterns within each network and identified each
177 network's inflection point, for each experimental condition. Moving from low-order networks
178 to higher-order networks, we found that decoding accuracy tended to increase, particularly in
179 the higher-order experimental conditions (Fig. 4D, E). This suggests that higher-order networks
180 may carry more content-relevant or stimulus-driven "information." We found no clear trends
181 in the proportions of components required to achieve 5% decoding accuracy across networks or
182 conditions (Fig. 4F).

183 In addition to examining different networks in isolation, we wondered about the general
184 structure of the full-brain (i.e., potentially multi-network) activity patterns reflected by different
185 principal components across different experimental conditions. As shown in Figure 5, we used
186 Neurosynth (Rubin et al., 2017) to identify, for each component, the associations with each of
187 80 themes (see *Reverse inference*). In general, the first principal components across all of the
188 experimental conditions tended to weight most heavily on themes related to cognitive control,
189 memory, language processing, attention, and perception. Other components appeared to vary
190 more across conditions.

191 To gain further insights into which brain functions might be most closely associated with

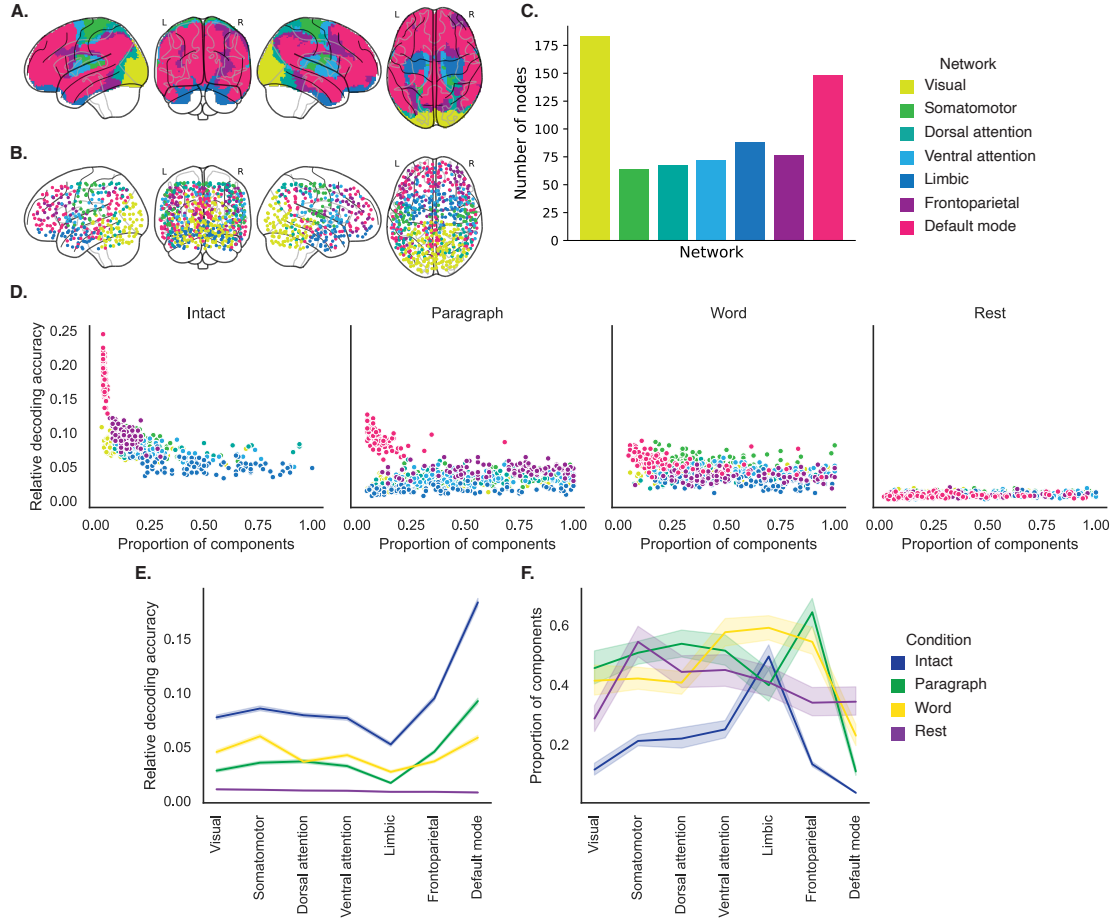


Figure 4: Network-specific decoding accuracy and compression. **A. Network parcellation map.** The glass brain displays the location of each of seven networks identified by Yeo et al. (2011). **B. Node labels.** We assigned network labels to each of 700 Hierarchical Topographic Factor Analysis-derived nodes (see *Hierarchical topographic factor analysis (HTFA)*). For each node, we evaluated its radial basis function (RBF) at the locations of every voxel in the parcellation map displayed in Panel A. We summed up these RBF weights separately for the voxels in each network. We defined each node's network label as its highest-weighted network across all voxels. **C. Per-network node counts.** The bar plot displays the total number of HTFA-derived nodes assigned to each network. **D. Informativeness versus compressibility by network and condition.** Each dot corresponds to a single cross validation run. The dots' coordinates denote the minimum proportion of components (relative to the number of nodes in the given network) required to achieve at least 5% corrected decoding accuracy (x -coordinate; for the rest condition these proportions are estimated using the peak decoding accuracies) and peak (corrected) decoding accuracy (y -coordinate). We repeated the analysis separately for each network (color) and experimental condition (column). **E. Informativeness by network.** For each network, sorted (roughly) from lower-order networks on the left to higher-order networks on the right, the curves display the peak (corrected) decoding accuracy for each experimental condition (color). **F. Compressibility by network.** For each network, the curves display the proportion of components (relative to the total possible number of components displayed in Panel C) required to achieve at least 5% decoding accuracy (or, for the rest condition, peak decoding accuracy, as described above). Error ribbons in Panels E and F denote 95% bootstrap-estimated confidence intervals.

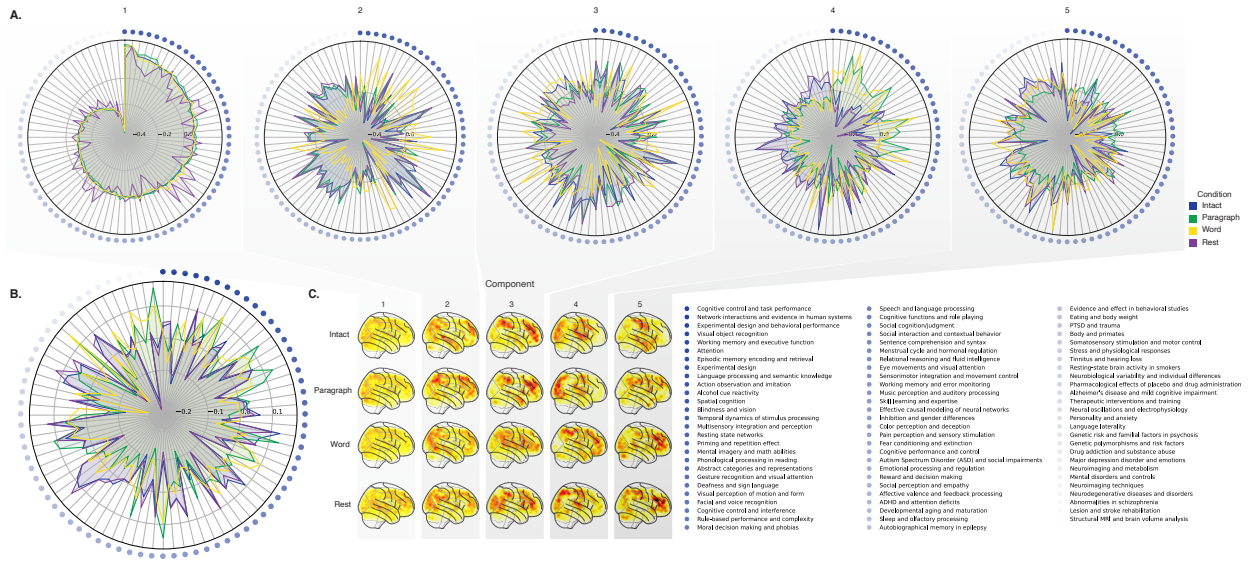


Figure 5: Neurosynth topic weightings by component. We used a reverse inference procedure (see *Reverse inference*) to estimate the correspondences between brain images and a set of 80 topics derived from the Neurosynth database of neuroimaging articles (Rubin et al., 2017). **A. Topic correlations by component.** For each of the top five highest-weighted principal components (columns) derived from each experimental condition (colors), the radar plots display the correlations between the component images and the per-topic images derived for each topic (topic identities are denoted by the blue dots; a legend for the topic labels is in the lower right of the figure). An annotated list of the top-weighted topics for each component and condition may be found in Figure S2 and the top-weighted terms for each topic may be found in Table S1. **B. Topic correlations averaged across components.** The radar plot is in the same format as the plots in Panel A, but here we display the per-condition average correlations across the top five components (for each condition) reflected in Panel A. **C. Component images.** Each plot displays a right sagittal view of a glass brain projection of the top five principal components (columns) for each experimental conditions (rows). Additional projections for each component may be found in Figure S3.

192 the top-weighted components from each experimental condition, we manually grouped each
193 Neurosynth-derived topic into a smaller set of core cognitive functions. Separately for each com-
194 ponent, we computed the average weightings across all topics that were tagged as being associated
195 with each of these cognitive functions (Figs. 6A, S5A). To help visualize these associations, we used
196 the patterns of associations for each component to construct graphs whose nodes were experimen-
197 tal conditions and cognitive functions (Figs. 6B, S5B). We also computed correlations between the
198 sets of per-topic weightings from each of the top-weighted components from each experimental
199 condition (Fig. 6C, D) and between the brain maps for each condition's components (Fig. S5C, D).
200 Taken together, we found that each component appeared to weight on a fundamental set of cogni-
201 tive functions that varied by experimental condition. For example, the top principal components
202 from every condition weighted similarly on the full set of Neurosynth topics (Fig. 5A) and cognitive
203 functions (Figs. 6A, B and S5 A, B), suggesting that these components might reflect a set of functions
204 or activity patterns that are common across all conditions. The second components' weightings
205 were similar across the intact, paragraph, and rest conditions (highest-weighted functions: cog-
206 nitive control, memory, social cognition, and resting state), but different for the word condition
207 (highest-weighted functions: sensory perception and cognitive control). The fourth components'
208 weighting grouped the paragraph and word conditions (highest-weighted functions: memory,
209 language processing, and cognitive control) and the intact and rest conditions (highest-weighted
210 functions: emotion, social cognition). We also used ChatGPT (OpenAI, 2023) to sort the list of
211 manually tagged cognitive functions from lowest-level to highest-level (Tab. S2, Fig. 6E; also see
212 *Ranking cognititive processes*). We found that higher-level functions tended to be weighted on more
213 heavily by top components from the intact and paragraph conditions than lower-level functions.
214 The top components from the word condition showed the opposite tendency, whereby *lower*-level
215 functions tended to be weighted on more heavily than higher-level functions. The components
216 from the rest condition showed almost no differences in the weights associated with high-level
217 versus low-level functions.

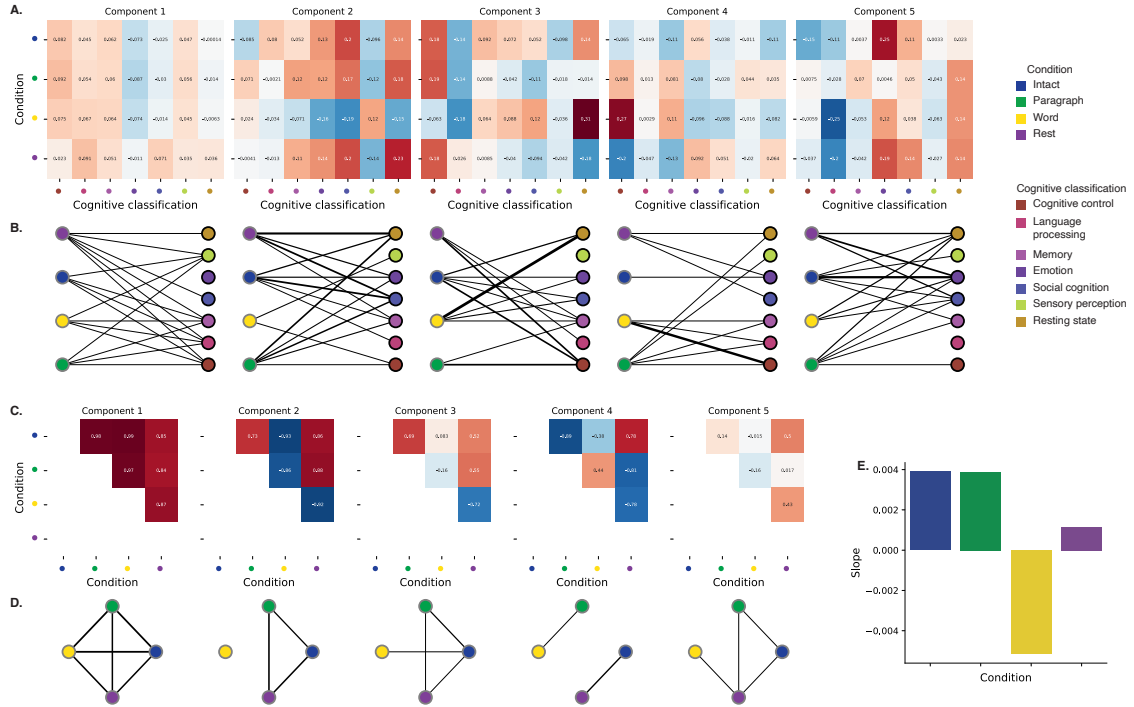


Figure 6: Summary of functions associated with top-weighted components by condition. A. Top-weighted topics by condition. Here we display per-condition (rows, indicated by colored dots) topic correlations, averaged across topics that pertain to each of several broad cognitive functions (columns within each sub-panel, indicated by colored dots). Each sub-panel reflects correlations for the components indicated in the panel titles. A legend for the condition and several core cognitive function classifications is displayed in the lower right of the figure. Table S1 provides a list of each topic's top-weighted terms, along with each topic's manually labeled cognitive classification. A full list of the topics most highly associated with each component may be found in Figure S2. **B. Associations between per-condition components and cognitive functions.** The network plots denote positive average correlations between the component images for each condition (gray-outlined dots on the left sides of each network; colors denote conditions) and topic-specific brain maps associated with each indicated cognitive function (black-outlined dots on the right sides of each network; colors denote cognitive functions). The line thicknesses are proportional to the correlation values (correlation coefficients are noted in the heatmaps in Panel A). **C. Correlations between each principal component, by condition.** The heatmaps display the correlations between the brain maps (Fig. S3) for each principal component (sub-panel), across each pair of conditions (rows and columns of each sub-panel's matrix, indicated by colored dots). **D. Associations between per-condition components, by component.** Each sub-panel's network plot summarizes the pattern of correlations between the n^{th} top-weighted principal components (sub-panel) for each experimental condition (gray-outlined dots). The line thicknesses are proportional to the correlation values (correlation coefficients are noted in the heatmaps in Panel C). **E. Change in weights by condition.** The bar heights reflect the slopes of regression lines, fit separately to the top five components from each condition, between the ChatGPT-derived “rank” of each cognitive classification and the correlations between the component and topic maps associated with cognitive processes at the given rank (see *Ranking cognitive processes*). Also see Fig. S5 for additional information.

218 **Discussion**

219 We examined fMRI data collected as participants listened to an auditory recording of a story, scram-
220 bled recordings of the story, or underwent a resting state scan. We found that cognitively richer
221 stimuli evoked more reliable (i.e., consistent across people) and information rich brain activity pat-
222 terns. The brain patterns evoked by cognitively richer stimuli were also more compressible, in that
223 each individual component provided more “signal” to temporal decoders relative to components
224 of data from less cognitively rich conditions (Fig. 2). Over time (e.g., as the experiment progressed),
225 these phenomena were strengthened. Specifically, across story segments, data from more cogni-
226 tively rich conditions became more informative and compressible, and data from less cognitively
227 rich conditions became *less* informative and compressible (Fig. 3). We also repeated these analyses
228 separately for different brain networks. We found that networks traditionally associated with
229 higher-level cognitive functions tended to provide more informative brain patterns than networks
230 traditionally associated with lower level cognitive functions (Fig. 4). Finally, we examined the most
231 dominant components of the brain activity patterns from each experimental condition. We used a
232 reverse inference approach (Rubin et al., 2017) to identify the terms in the neuroimaging literature
233 most commonly associated with the corresponding maps. As summarized in Figure 6E, we found
234 that the intact and paragraph conditions tended to weight on higher-level cognitive processes
235 more than lower-level cognitive processes, whereas the word condition weighted on lower-level
236 processes more than higher-level processes and the rest condition showed no difference in high-
237 level versus low-level weighting. Taken together, our findings indicate that the informativeness
238 and compressibility of our brain activity patterns are task-dependent, and these properties change
239 systematically with factors like cognitive richness and depth of processing.

240 Our explorations of informativeness and compressibility are related to a much broader litera-
241 ture on the correlational and causal structure of brain activity patterns (Adachi et al., 2012; Bassett
242 & Sporns, 2017; Brovelli et al., 2004; Bullmore & Sporns, 2009; Dhamala et al., 2008; Korzeniewska
243 et al., 2008; Owen et al., 2021; Preti et al., 2017; Rogers et al., 2007; Rubinov & Sporns, 2010; Size-
244 more et al., 2018; Smith, Beckmann, et al., 2013; Smith, Vidaurre, et al., 2013; Sporns & Betzel, 2016;
245 Sporns & Honey, 2006; Sporns & Zwi, 2004; Srinivasan et al., 2007; Tomasi & Volkow, 2011; Yeo
246 et al., 2011). Correlations or causal associations between different brain regions simultaneously

247 imply that full-brain activity patterns will be compressible and also that those activity patterns
248 will contain redundancies. For example, the extent to which activity patterns at one brain area can
249 be inferred or predicted from activity patterns at other areas (e.g., Owen et al., 2020; Scangos et al.,
250 2021), reflects overlap in the information available in or represented by those brain areas. If brain
251 patterns in one area are recoverable using brain patterns in another area, then a “signal” used to
252 convey the activity patterns could be compressed by removing the recoverable activity. Predictable
253 (and therefore redundant) brain activity patterns are also more robust to signal corruption. For
254 example, even if the activity patterns at one region are unreadable or unreliable at a given moment,
255 that unreliability could be compensated for by other regions’ activity patterns that were predictive
256 of the unreliable region.

257 Our findings that informativeness and compressibility change with task demands may follow
258 from task-dependent changes in full-brain correlation patterns. A number of prior studies have
259 found that so-called “functional connectivity” (i.e., correlational) patterns vary reliably across
260 tasks, events, and situations (Cole et al., 2014; Owen et al., 2021; Simony et al., 2016; Smith et
261 al., 2009). By examining how these task-dependent changes in correlations affect informativeness
262 and compressibility, our work suggests a potential reason why the statistical structure of brain
263 activity patterns might vary with cognitive task or with cognitive demands. For lower-level tasks,
264 or for tasks that require relatively little “deep” cognitive processing, our brains may optimize
265 activity patterns for robustness and redundancy over expressiveness, for example to maximize
266 reliability. For higher-level tasks, or for tasks that require deeper cognitive processing, our brains
267 may sacrifice some redundancy in favor of greater expressiveness.

268 In the information theory sense (Shannon, 1948), when a signal is transmitted using a fixed
269 alphabet of “symbols,” the information rate decreases as the signal is compressed (e.g., fewer sym-
270 bols transmitted per unit time, using an alphabet with fewer symbols, etc.). Our finding that each
271 individual brain component (symbol) becomes more informative as cognitive richness increases
272 suggests that the “alphabet” of brain activity patterns is also task-dependent. Other work suggests
273 that the representations that are *reflected* by brain activity patterns may also change with task de-
274 mands. For example, our brains may represent the same perceptual stimulus differently depending
275 on which aspects of the stimulus or which combinations of features are task-relevant (Mack et al.,
276 2020).

277 Different brain networks also varied in how informative and compressible their activity pat-
278 terns were across experimental conditions (e.g., Fig. 4). This might follow from evolutionary
279 optimizations that reflect the relevant constraints or demands placed on those networks. One
280 possibility is that cortex is organized in a hierarchy of networks “concerned with” or selective to
281 different levels of processing or function. To the extent that different levels of processing (e.g.,
282 low-level sensory processing versus “deeper” higher-level processing) reflect different stimulus
283 timescales (e.g., Manning, 2020), the network differences we observed might also relate to the
284 timescales at which each network is maximally sensitive (Baldassano et al., 2017; Hasson et al.,
285 2008; Lerner et al., 2011; Regev et al., 2018).

286 **Concluding remarks**

287 Cognitive neuroscientists are still grappling with basic questions about the fundamental “rules”
288 describing how our brains respond, and about how brain activity patterns and the associated
289 underlying cognitive representations and computations are linked. We identified two aspects of
290 brain activity patterns, informativeness and compressibility, that appear to change systematically
291 with task demands and across brain networks. Our work helps to clarify how the “neural code”
292 might be structured, and how the code might vary across tasks and brain areas.

293 **Methods**

294 We measured properties of recorded neuroimaging data under different task conditions that varied
295 systematically in cognitive engagement and depth of processing. We were especially interested in
296 how *informative* and *compressible* the activity patterns were under these different conditions (Fig. 1).

297 **Functional neuroimaging data collected during story listening**

298 We examined an fMRI dataset collected by Simony et al. (2016) that the authors have made publicly
299 available at arks.princeton.edu/ark:/88435/dsp015d86p269k. The dataset comprises neuroimaging
300 data collected as participants listened to an audio recording of a story (intact condition; 36 par-
301 ticipants), listened to temporally scrambled recordings of the same story (17 participants in the
302 paragraph-scrambled condition listened to the paragraphs in a randomized order and 36 in the

303 word-scrambled condition listened to the words in a randomized order), or lay resting with their
304 eyes open in the scanner (rest condition; 36 participants). Full neuroimaging details may be found
305 in the original paper for which the data were collected (Simony et al., 2016). Procedures were
306 approved by the Princeton University Committee on Activities Involving Human Subjects, and by
307 the Western Institutional Review Board (Puyallup, WA). All subjects were native English speakers
308 with normal hearing and provided written informed consent.

309 **Hierarchical topographic factor analysis (HTFA)**

310 Following our prior related work, we used HTFA (Manning et al., 2018) to derive a compact
311 representation of the neuroimaging data. In brief, this approach approximates the timeseries
312 of voxel activations (44,415 voxels) using a much smaller number of radial basis function (RBF)
313 nodes (in this case, 700 nodes, as determined by an optimization procedure; Manning et al., 2018).
314 This provides a convenient representation for examining full-brain activity patterns and network
315 dynamics. All of the analyses we carried out on the neuroimaging dataset were performed in
316 this lower-dimensional space. In other words, each participant's data matrix was a number-of-
317 timepoints (T) by 700 matrix of HTFA-derived factor weights (where the row and column labels
318 were matched across participants). Code for carrying out HTFA on fMRI data may be found as
319 part of the BrainIAK toolbox (Capota et al., 2017; Kumar et al., 2021), which may be downloaded
320 at brainiak.org.

321 **Principal components analysis (PCA)**

322 We applied group PCA (Smith et al., 2014) separately to the HTFA-derived representations of the
323 data (i.e., factor loadings) from each experimental condition. Specifically, for each condition, we
324 considered the set of all participants' T by 700 factor weight matrices. We used group PCA to project
325 these 700-dimensional matrices into a series of shared k -dimensional spaces, for $k \in \{3, 4, 5, \dots, 700\}$.
326 This yielded a set of number-of-participants matrices, each with T rows and k columns.

327 **Temporal decoding**

328 We sought to identify neural patterns that reflected participants' ongoing cognitive processing of
329 incoming stimulus information. As reviewed by Simony et al. (2016), one way of homing in on
330 these stimulus-driven neural patterns is to compare activity patterns across individuals. In partic-
331 ular, neural patterns will be similar across individuals to the extent that the neural patterns under
332 consideration are stimulus-driven, and to the extent that the corresponding cognitive representa-
333 tions are reflected in similar spatial patterns across people (Simony & Chang, 2020). Following this
334 logic, we used an across-participant temporal decoding test developed by Manning et al. (2018) to
335 assess the degree to which different neural patterns reflected ongoing stimulus-driven cognitive
336 processing across people. The approach entails using a subset of the data to train a classifier to
337 decode stimulus timepoints (i.e., moments in the story participants listened to) from neural pat-
338 terns. We use decoding (forward inference) accuracy on held-out data, from held-out participants,
339 as a proxy for the extent to which the inputted neural patterns reflected stimulus-driven cognitive
340 processing in a similar way across individuals.

341 **Forward inference and decoding accuracy**

342 We used an across-participant correlation-based classifier to decode which stimulus timepoint
343 matched each timepoint's neural pattern. For a given value of k (i.e., number of principal compo-
344 nents), we first used group PCA to project the data from each condition into a shared k -dimensional
345 space. Next, we divided the participants into two groups: a template group, $\mathcal{G}_{\text{template}}$ (i.e., training
346 data), and a to-be-decoded group, $\mathcal{G}_{\text{decode}}$ (i.e., test data). We averaged the projected data within
347 each group to obtain a single T by k matrix for each group. Next, we correlated the rows of the two
348 averaged matrices to form a T by T decoding matrix, Λ . In this way, the rows of Λ reflected time-
349 points from the template group, while the columns reflected timepoints from the to-be-decoded
350 group. We used Λ to assign temporal labels to each timepoint (row) from the test group's ma-
351 trix, using the row of the training group's matrix with which it was most highly correlated. We
352 repeated this decoding procedure, but using $\mathcal{G}_{\text{decode}}$ as the template group and $\mathcal{G}_{\text{template}}$ as the
353 to-be-decoded group. Given the true timepoint labels (for each group), we defined the decoding
354 accuracy as the average proportion of correctly decoded timepoints, across both groups (where

355 chance performance is $\frac{1}{T}$). In Figures 2 and 3 we report the decoding accuracy for each condition
356 and value of k , averaged across $n = 100$ cross validation folds.

357 **Reverse inference**

358 To help interpret the brain activity patterns we found within the contexts of other studies, we
359 created summary maps of each principal component, for each experimental condition. Each
360 principal component comprises 700 “weights” on each of the HTFA-derived RBF nodes (see
361 *Hierarchical Topographic Factor Analysis*). For each node, we evaluated its RBF at the locations of
362 every voxel in the standard 2 mm MNI152 template brain and multiplied the RBF by the node’s
363 weight. The sum of these weighted RBF activation maps provides a full-brain image, in MNI152
364 space, of the given principal component (Fig. S3).

365 Next, we considered 80 topics estimated using Latent Dirichlet Allocation (Blei et al., 2003)
366 applied to 9,204 functional neuroimaging articles in the Neurosynth database (Rubin et al., 2017).
367 The topics, as well as associated brain maps identified using Neurosynth, were identified and
368 reported in several prior studies (Chen et al., 2020; Fox et al., 2014; Sul et al., 2017). The topic
369 labels for each topic were generated automatically with the following ChatGPT (chat.openai.com)
370 prompt: “Please help me come up with intuitive labels for topic topics I found by fitting a topic
371 model to thousands of neuroscience and psychology articles. I’ll paste in the top 10 highest-
372 weighted words for each topic, and I’d like you to respond with a suggested label. For each topic,
373 please respond with just the topic label and no other formatting or text. Here are the next topic’s
374 top words:” followed by a comma-separated list of the given topic’s top-weighted words reflected
375 in the Table S1. For some topics, ChatGPT responded with a longer-form response rather than a
376 concise topic label. In these instances, on a case-by-case basis, we used a second follow-up prompt
377 to achieve the given topic’s label: “Could you please come up with a more concise label for that
378 topic?”. We then manually identified a set of 11 cognitive labels that were intended to encapsulate
379 a representative range of widely studied low-level and high-level cognitive functions. In choosing
380 the set of cognitive labels, we jointly considered each topic’s ChatGPT-derived topic label, along
381 with the top-weighted words for the topic. We attempted to generate a concise set of labels that
382 still spanned the full set of cognitive functions reflected across the 80 topics. Topics that appeared

383 unrelated to specific cognitive functions (e.g., topics related to specific methods or clinical themes)
384 are designated with dashes in Table S1.

385 Finally, following an approach used in several prior studies (Chen et al., 2020; Fox et al., 2014;
386 Sul et al., 2017) we treated the correlation between a given component's brain map and each
387 topic's brain map as a reflection of how much the component was reflective of the given topic.
388 This resulted in a set of 80 "weights" (correlation coefficients) for each component's brain map,
389 with one weight per Neurosynth-derived topic.

390 **Ranking cognitive processes**

391 We manually identified 11 cognitive labels spanning the set of 80 Neurosynth-derived topics:
392 cognitive control, language processing, memory, emotion, social cognition, spatial cognition, at-
393 tention, reward, sensory perception, motor control, and resting state. We then used ChatGPT
394 to automatically "rank" the processes from high-level to low-level using the following prompt:
395 "Please rank these cognitive processes from highest-level to lowest-level, where higher values
396 indicate higher-order or higher-level processes. Return the result as a csv file with a header row
397 and two columns: 'Cognitive label' and 'Rank'. Here are the processes: cognitive control, lan-
398 guage processing, memory, emotion, social cognition, spatial cognition, attention, reward, sensory
399 perception, motor control, resting state". Table S2 displays the output. We used these labels
400 in the analysis presented in Figure 6E to help summarize difference in topic weightings across
401 experimental conditions.

402 **Data and code availability**

403 All of the code used to produce the figures and results in this manuscript, along with links to the
404 corresponding data, may be found at github.com/ContextLab/pca_paper.

405 **Acknowledgements**

406 We acknowledge discussions with Rick Betzel, Luke Chang, Emily Finn, and Jim Haxby. Our
407 work was supported in part by NSF CAREER Award Number 2145172 to J.R.M. The content is

408 solely the responsibility of the authors and does not necessarily represent the official views of our
409 supporting organizations. The funders had no role in study design, data collection and analysis,
410 decision to publish, or preparation of the manuscript.

411 Author contributions

412 Conceptualization: J.R.M. and L.L.W.O. Methodology: J.R.M. and L.L.W.O. Implementation: L.L.W.O.
413 Analysis: L.L.W.O. Writing, Reviewing, and Editing: J.R.M. and L.L.W.O. Supervision: J.R.M.

414 References

- 415 Adachi, Y., Osada, T., Sporns, O., Watanabe, T., Matsui, T., Miyamoto, K., & Miyashita, Y.
416 (2012). Functional connectivity between anatomically unconnected areas is shaped by collective
417 network-level effects in the macaque cortex. *Cerebral Cortex*, 22(7), 1586–1592.
- 418 Alvarez, S. A. (2002). *An exact analytical relation among recall, precision, and classification accuracy in*
419 *information retrieval* (Technical Report No. BCCS-02-01). Boston College.
- 420 Baldassano, C., Chen, J., Zadbood, A., Pillow, J. W., Hasson, U., & Norman, K. A. (2017). Discov-
421 ering event structure in continuous narrative perception and memory. *Neuron*, 95(3), 709–721.
- 422 Bassett, D. S., & Sporns, O. (2017). Network neuroscience. *Nature Neuroscience*, 20(3), 353–364.
- 423 Blei, D. M., Ng, A. Y., & Jordan, M. I. (2003). Latent dirichlet allocation. *Journal of Machine Learning*
424 *Research*, 3, 993–1022.
- 425 Brovelli, A., Ding, M., Ledberg, A., Chen, Y., Nakamura, R., & Bressler, S. (2004). Beta oscillations in
426 a large-scale sensorimotor cortical network: directional influences revealed by Granger causality.
427 *Proceedings of the National Academy of Sciences, USA*, 101(26), 9849–9854.
- 428 Bullmore, E., & Sporns, O. (2009). Complex brain networks: graph theoretical analysis of structural
429 and functional systems. *Nature Reviews Neuroscience*, 10(3), 186–198.
- 430 Capota, M., Turek, J., Chen, P.-H., Zhu, X., Manning, J. R., Sundaram, N., ... Shin, Y. S. (2017).
431 *Brain imaging analysis kit*.

- 432 Chen, P.-H. A., Jolly, E., Cheong, J. H., & Chang, L. J. (2020). Intersubject representational
433 similarity analysis reveals individual variations in affective experience when watching erotic
434 movies. *NeuroImage*, 216(116851), doi.org/10.1016/j.neuroimage.2020.116851.
- 435 Cole, M. W., Bassett, D. S., Power, J. D., Braver, T. S., & Petersen, S. E. (2014). Intrinsic and
436 task-evoked network architectures of the human brain. *Neuron*, 83(1), 238–251.
- 437 Dhamala, M., Rangarajan, G., & Ding, M. (2008). Analyzing information flow in brain networks
438 with nonparametric Granger causality. *NeuroImage*, 41(2), 354–362.
- 439 Finn, E. S., Scheinost, D., Finn, D. M., Shen, X., Papademetris, X., & Constable, R. T. (2017).
440 Can brain state be manipulated to emphasize individual differences in functional connectivity.
441 *NeuroImage*, 160, 140–151.
- 442 Finn, E. S., Shen, X., Scheinost, D., Rosenberg, M. D., Huang, J., Chun, M. M., ... Constable, R. T.
443 (2015). Functional connectome fingerprinting: identifying individuals using patterns of brain
444 connectivity. *Nature Neuroscience*, 18, 1664–1671.
- 445 Fox, A. S., Chang, L. J., Gorgolewski, K. J., & Yarkoni, T. (2014). Bridging psychology and
446 genetics using large-scale spatial analysis of neuroimaging and neurogenetic data. *bioRxiv*,
447 doi.org/10.1101/012310.
- 448 Glerean, E., Salmi, J., Lahnakoski, J. M., Jääskeläinen, I. P., & Sams, M. (2012). Functional magnetic
449 resonance imaging phase synchronization as a measure of dynamic functional connectivity.
450 *Brain Connectivity*, 2(2), 91–101.
- 451 Gratton, C., Laumann, T. O., Nielsen, A. N., Greene, D. J., Gordon, E. M., Gilmore, A. W., ...
452 Petersen, S. E. (2018). Functional brain networks are dominated by stable group and individual
453 factors, not cognitive or daily variation. *Neuron*, 98(2), 439–452.
- 454 Hasson, U., Yang, E., Vallines, I., Heeger, D. J., & Rubin, N. (2008). A hierarchy of temporal
455 receptive windows in human cortex. *The Journal of Neuroscience*, 28(10), 2539–2550.
- 456 Korzeniewska, A., Crainiceanu, C. M., Kus, R., Franaszczuk, P. J., & Crone, N. E. (2008). Dynamics
457 of event-related causality in brain electrical activity. *Human Brain Mapping*, 29(10).

- 458 Kumar, M., Anderson, M. J., Antony, J. W., Baldassano, C., Brooks, P. P., Cai, M. B., ... Norman,
459 K. A. (2021). BrainIAK: the brain image analysis kit. *Aperture*, *In press*.
- 460 Lerner, Y., Honey, C. J., Silbert, L. J., & Hasson, U. (2011). Topographic mapping of a hierarchy of
461 temporal receptive windows using a narrated story. *The Journal of Neuroscience*, 31(8), 2906–2915.
- 462 Mack, M. L., Preston, A. R., & Love, B. C. (2020). Ventromedial prefrontal cortex compressesion
463 during concept learning. *Nature Communications*, 11(46), doi.org/10.1038/s41467-019-13930-8.
- 464 Manning, J. R. (2020). Context reinstatement. In M. J. Kahana & A. D. Wagner (Eds.), *Handbook of
465 human memory*. Oxford University Press.
- 466 Manning, J. R., Zhu, X., Willke, T. L., Ranganath, R., Stachenfeld, K., Hasson, U., ... Norman,
467 K. A. (2018). A probabilistic approach to discovering dynamic full-brain functional connectivity
468 patterns. *NeuroImage*, 180, 243–252.
- 469 Norman, K. A., Polyn, S. M., Detre, G. J., & Haxby, J. V. (2006). Beyond mind-reading: multi-voxel
470 pattern analysis of fMRI data. *Trends in Cognitive Sciences*, 10(9), 424–430.
- 471 OpenAI. (2023, March). *ChatGPT*. Personal communication.
- 472 Owen, L. L. W., Chang, T. H., & Manning, J. R. (2021). High-level cognition during story listening is
473 reflected in high-order dynamic correlations in neural activity patterns. *Nature Communications*,
474 12(5728), doi.org/10.1038/s41467-021-25876-x.
- 475 Owen, L. L. W., Muntianu, T. A., Heusser, A. C., Daly, P., Scangos, K. W., & Manning, J. R. (2020). A
476 Gaussian process model of human electrocorticographic data. *Cerebral Cortex*, 30(10), 5333–5345.
- 477 Preti, M. G., Bolton, T. A. W., & Van De Ville, D. (2017). The dynamic functional connectome:
478 state-of-the-art and perspectives. *NeuroImage*, 160, 41–54.
- 479 Regev, M., Simony, E., Lee, K., Tan, K. M., Chen, J., & Hasson, U. (2018). Propagation of information
480 along the cortical hierarchy as a function of attention while reading and listening to stories.
481 *Cerebral Cortex*.
- 482 Rogers, B. P., Morgan, V. L., Newton, A. T., & Gore, J. C. (2007). Assessing functional connectivity
483 in the human brain by fMRI. *Magnetic Resonance Imaging*, 25(11), 1347–1357.

- 484 Rubin, T. N., Kyojo, O., Gorgolewski, K. J., Jones, M. N., Poldrack, R. A., & Yarkoni, T. (2017).
485 Decoding brain activity using a large-scale probabilistic functional-anatomical atlas of human
486 cognition. *PLoS Computational Biology*, 13(10), e1005649.
- 487 Rubinov, M., & Sporns, O. (2010). Complex network measures of brain connectivity: uses and
488 interpretations. *NeuroImage*, 52, 1059–1069.
- 489 Scangos, K. W., Khambhati, A. N., Daly, P. M., Owen, L. L. W., Manning, J. R., Ambrose, J. B.,
490 ... Chang, E. F. (2021). Biomarkers of depression symptoms defined by direct intracranial
491 neurophysiology. *Frontiers in Human Neuroscience*, In press.
- 492 Shannon, C. E. (1948). A mathematical theory of communication. *Bell System Technical Journal*,
493 27(3), 379–423.
- 494 Simony, E., & Chang, C. (2020). Analysis of stimulus-induced brain dynamics during naturalistic
495 paradigms. *NeuroImage*, 216, 116461.
- 496 Simony, E., Honey, C. J., Chen, J., & Hasson, U. (2016). Dynamic reconfiguration of the default
497 mode network during narrative comprehension. *Nature Communications*, 7(12141), 1–13.
- 498 Sizemore, A. E., Giusti, C., Kahn, A., Vettel, J. M., Betzel, R. F., & Bassett, D. S. (2018). Cliques and
499 cavities in the human connectome. *Journal of Computational Neuroscience*, 44(1), 115–145.
- 500 Smith, S. M., Beckmann, C. F., Andersson, J., Auerbach, E. J., Bijsterbosch, J., Douaud, G., ...
501 Glasser, M. F. (2013). Resting-state fMRI in the Human Connectome Project. *NeuroImage*, 80,
502 144–168.
- 503 Smith, S. M., Fox, P. T., Miller, K. L., Glahn, D. C., Fox, P. M., Mackay, C. E., ... Beckmann,
504 C. F. (2009). Correspondence of the brain's functional architecture during activation and rest.
505 *Proceedings of the National Academy of Sciences, USA*, 106(31), 13040–13045.
- 506 Smith, S. M., Hyvärinen, A., Varoquaux, G., Miller, K. L., & Beckmann, C. F. (2014). Group-PCA
507 for very large fMRI datasets. *NeuroImage*, 101, 738–749.

- 508 Smith, S. M., Vidaurre, D., Beckmann, C. F., Glasser, M. F., Jenkinson, M., Miller, K. L., ... Van
509 Essen, D. C. (2013). Functional connectomics from resting-state fMRI. *Trends in Cognitive Sciences*,
510 17(12), 666–682.
- 511 Sporns, O., & Betzel, R. F. (2016). Modular brain networks. *Annual Review of Psychology*, 67,
512 613–640.
- 513 Sporns, O., & Honey, C. J. (2006). Small worlds inside big brains. *Proceedings of the National Academy
514 of Sciences, USA*, 103(51), 19219–19220.
- 515 Sporns, O., & Zwi, J. D. (2004). The small world of the cerebral cortex. *Neuroinformatics*, 2(2),
516 145–162.
- 517 Srinivasan, R., Winter, W. R., Ding, J., & Nunez, P. L. (2007). EEG and MEG coherence: Measures of
518 functional connectivity at distinct spatial scales of neocortical dynamics. *Journal of Neuroscience
519 Methods*, 166, 41–52.
- 520 Sul, S., Güroğlu, B., Crone, E. A., & Chang, L. J. (2017). Medial prefrontal cortical thinning
521 mediates shifts in other-regarding preferences during adolescence. *Scientific Reports*, 7(8510),
522 doi.org/10.1038/s41598-017-08692-6.
- 523 Tomasi, D., & Volkow, N. D. (2011). Association between functional connectivity hubs and brain
524 networks. *Cerebral Cortex*, 21, 2003–2013.
- 525 Yeo, B. T. T., Krienen, F. M., Sepulcre, J., Sabuncu, M. R., Lashkari, D., Hollinshead, M., ... Buckner,
526 R. L. (2011). The organization of the human cerebral cortex estimated by intrinsic functional
527 connectivity. *Journal of Neurophysiology*, 106(3), 1125–1165.